

Radiocarbon evidence for the stability of polar ocean overturning during the Holocene

Received: 29 November 2022

Accepted: 24 May 2023

Published online: 26 June 2023

 Check for updates

Tianyu Chen^{1,2}✉, Laura F. Robinson², Tao Li³, Andrea Burke⁴, Xu Zhang⁵, Joseph A. Stewart², Nicky J. White⁶ & Timothy D. J. Knowles⁷

Proxy-based studies have linked the pre-industrial atmospheric p_{CO_2} rise of ~20 ppmv in the mid- to late Holocene to an inferred increase in the Southern Ocean overturning and associated biogeochemical changes. However, the history of polar ocean overturning and ventilation through the Holocene remains poorly constrained, leaving important gaps in the assessment of the feedbacks between changes in ocean circulation and the carbon cycle in a warm climate state. The deep-ocean radiocarbon content, which provides a measure of ventilation, responds to circulation changes on centennial to millennial time scales. Here we present absolutely dated deep-sea coral radiocarbon records from the Drake Passage, between South America and Antarctica, and Reykjanes Ridge, south of Iceland, over the Holocene. Our data suggest that ventilation in the Antarctic circumpolar waters and North Atlantic Deep Water is surprisingly invariant within proxy uncertainties at our sampling resolution. Our findings indicate that long-term, large-scale polar ocean overturning has not been disturbed to a level resolvable by radiocarbon and is probably not responsible for the millennial atmosphere p_{CO_2} evolution through the Holocene. Instead, continuous nutrient and carbon redistribution within the water column following deglaciation, as well as changes in land organic carbon stock, might have regulated atmospheric CO_2 budget during this period.

The Holocene (-11.5 thousand years ago (ka) to the present) is the most recent warm interglacial and was characterized by a gradual decline in the Earth's axial tilt, increasing the precession index, waning continental ice sheets and changing greenhouse gas concentrations. Considerable millennial-scale variability has been found from various reconstructions under high-latitude surface ocean conditions, such as changing wind

strengths, sea-ice extent and fresh water flux^{1–6}. These climate forcings might in turn regulate meridional overturning circulations in the North Atlantic and Southern Ocean, which play a major role in deep-ocean ventilation and air–sea carbon cycling. Notably, atmospheric p_{CO_2} in the early Holocene exhibited a slight decrease by -5 ppmv from -11–6 ka and then increased by -20 ppmv from -6 ka to the pre-industrial period⁷.

¹State Key Laboratory for Mineral Deposits Research, School of Earth Sciences and Engineering and Frontiers Science Center for Critical Earth Material Cycling, Nanjing University, Nanjing, China. ²School of Earth Sciences, University of Bristol, Bristol, UK. ³State Key Laboratory of Palaeobiology and Stratigraphy, Nanjing Institute of Geology and Palaeontology, Chinese Academy of Sciences, Nanjing, China. ⁴School of Earth and Environmental Sciences, University of St Andrews, St Andrews, UK. ⁵Group of Alpine Paleocology and Human Adaptation (ALPHA), State Key Laboratory of Tibetan Plateau Earth System, Resources and Environment (TPESRE), Institute of Tibetan Plateau Research, Chinese Academy of Sciences, Beijing, China.

⁶Bullard Laboratories, Department of Earth Sciences, University of Cambridge, Cambridge, UK. ⁷School of Chemistry, University of Bristol, Bristol, UK.

✉e-mail: tianyuchen@nju.edu.cn

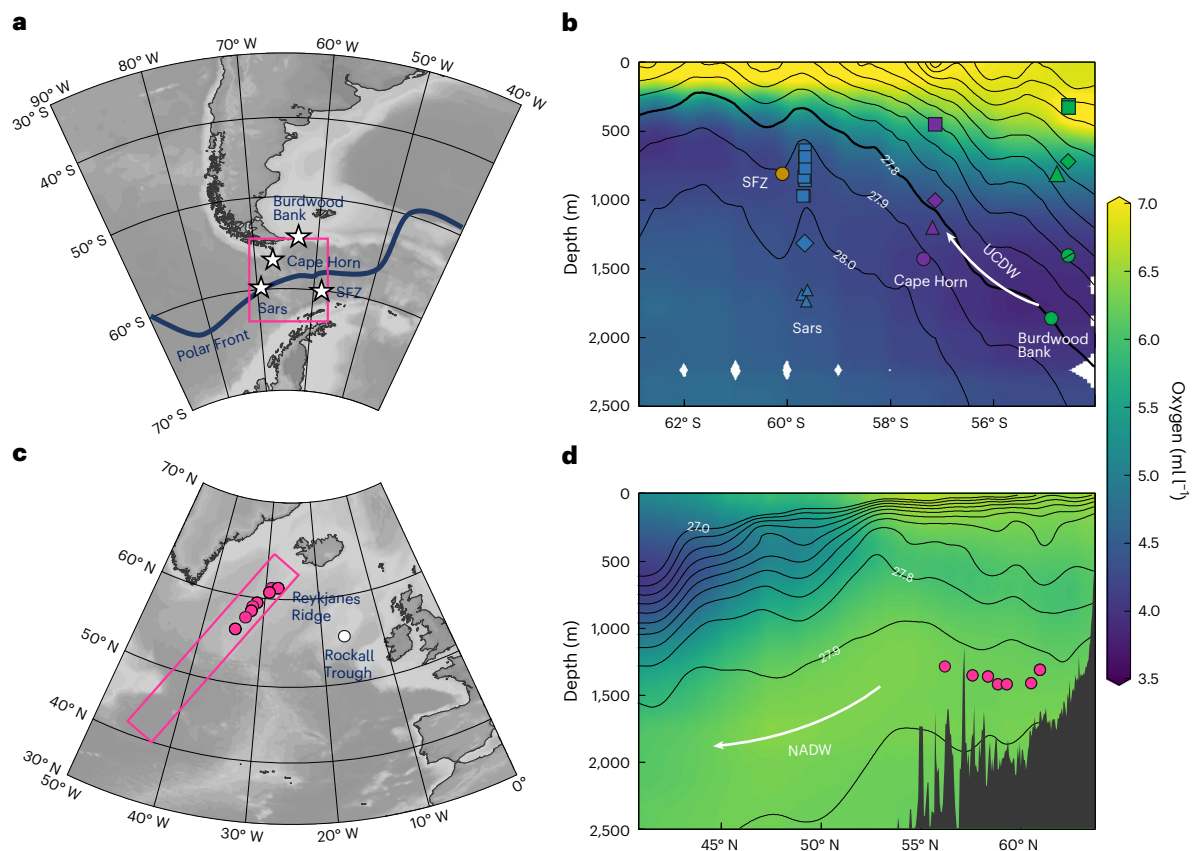


Fig. 1 | Locations of the samples in this study. **a**, Map of the Drake Passage, showing the Shackleton Fracture Zone (SFZ), Sars Seamount, Cape Horn and Burdwood Bank, where the deep-sea coral samples were collected. The dark blue line indicates the modern polar front. **b**, Depth–latitude section of the oxygen distribution in the Drake Passage. The sampling sites are labelled and colour coded (SFZ, yellow; Sars Seamount, blue; Cape Horn, purple; Burdwood Bank, green). The upwelling of UCDW is marked by the arrow. **c**, Map of the North Atlantic showing the locations of the Reykjanes Ridge samples for this study and

the Rockall Trough samples from the literature^{22,23}. **d**, Depth–latitude section of oxygen distribution in the North Atlantic, with pink points representing Reykjanes Ridge samples. The black lines with white numbers in **b** and **d** indicate the modern neutral density anomalies (GLODAPv2.2019; ref. 49). The southward-flowing NADW is marked by the arrow. Plotted with Ocean Data View (<https://odv.awi.de/>). Oxygen concentration data from WOCE09 (<https://odv.awi.de/data/ocean/world-ocean-atlas-2009/>).

In the North Atlantic, the history of Holocene overturning has been inferred from multiple approaches, such as reconstructions on bottom water flow speed^{8,9}, deep-water transport flux^{10,11} and mid- to high-latitude salinity/temperature anomalies^{12–14}. Nevertheless, existing reconstructions exhibit quite divergent trends, which might partly result from the fact that the Atlantic Meridional Overturning Circulation (AMOC) has different dynamic regimes and pathways¹⁵. In the Antarctic circumpolar system, detailed overturning and ventilation reconstructions over the Holocene have been hampered by the lack of suitable sedimentary archives. Moreover, consensus has not been reached on the position of the Southern Hemisphere westerlies^{2,3,5,16}, which impacts the Southern Ocean overturning and ventilation. The relationship between atmospheric p_{CO_2} and polar ocean overturning during the Holocene thus remains elusive.

Radiocarbon evolution reconstructed from deep-sea corals

Radiocarbon has been widely used as a ventilation and overturning proxy because it is dissolved in the surface ocean through air–sea exchange and is introduced into depths by deep-water formation¹⁷. As ^{14}C is radioactive, precise and accurate calendar ages are crucial for reliable reconstruction of ^{14}C evolution. The aragonite skeletons of deep-sea corals record ambient seawater ^{14}C during growth and their independent growth ages can be precisely determined via the uranium (U)-series disequilibrium method (Methods). We took the

approach of reconstructing ^{14}C evolution at different sites across the Drake Passage and Reykjanes Ridge, south of Iceland, through coupled U-series dating and ^{14}C analysis of deep-sea corals. The deep-sea corals of this study were recovered from Burdwood Bank, Cape Horn, Sars Seamount and the Shackleton Fracture Zone in the Drake Passage at a depth of ~ 0.3 – 1.9 km and from the Reykjanes Ridge at a depth of ~ 1.3 – 1.4 km (Fig. 1 and Methods).

The reconstructed $\Delta^{14}\text{C}$ (defined as $(F^{14}\text{C} \times e^{(\text{calenderage}/8,267)} - 1) \times 1,000$, where $F^{14}\text{C}$ is the fraction modern of the sample with blank and $\delta^{13}\text{C}$ correction) of different water masses in our records shows a gradual decrease over the past 10,000 years or so, following the trend of atmospheric radiocarbon reconstructed by IntCal20 (ref. 18), particularly for the samples from the Reykjanes Ridge (Fig. 2). These data also indicate distinctive $\Delta^{14}\text{C}$ values between different sites, with better ^{14}C ventilated signatures at shallower and northern sites of the Drake Passage. Intriguingly, the shallow depths at Sars Seamount show distinctively enriched ^{14}C signatures at ~ 9.6 ka, which are reproducible from two different samples from the same sampling site. To interpret radiocarbon in terms of overturning changes, it is necessary to account for the contribution of changing atmospheric $\Delta^{14}\text{C}$ on the initial ^{14}C content of deep waters at the time of their formation, as well as the atmospheric p_{CO_2} effect that impacts the air–sea carbon isotope exchange efficiency¹⁹. We therefore projected our ^{14}C data to the Marine20 calibration curve²⁰ (t_{proj}) as a proxy of deep-water ventilation age (Methods). Note that Marine20 represents the average ^{14}C concentration of the

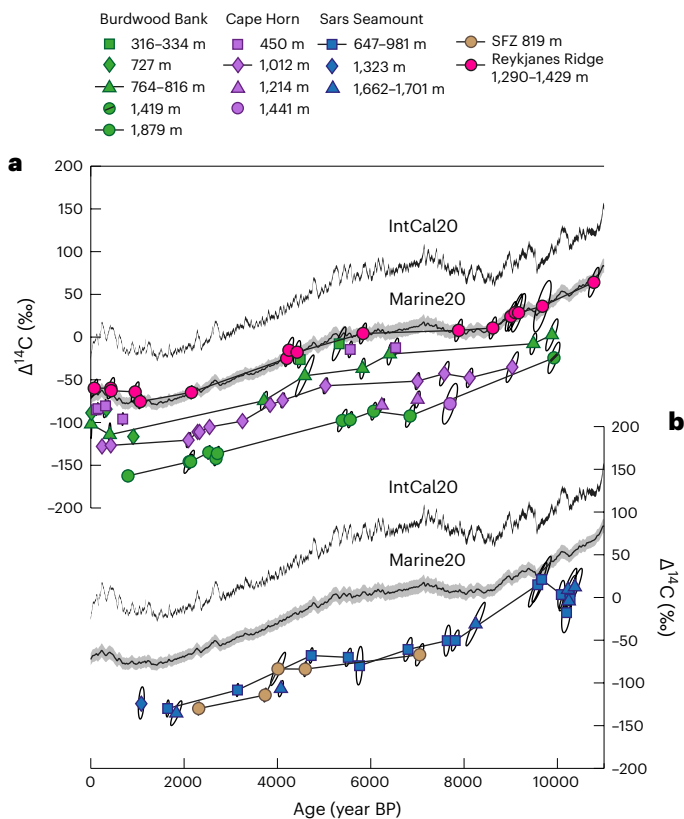


Fig. 2 | Reconstructed $\Delta^{14}\text{C}$ variability of different sites in this study. The symbols of the samples are the same as those shown in Fig. 1. $\pm 2\sigma$ error ellipses are also shown. IntCal20 represents the Northern Hemisphere atmospheric ^{14}C age calibration curve¹⁸, whereas Marine20 represents the non-polar marine ^{14}C age calibration curve²⁰. The shadings of Marine20 represent $\pm 2\sigma$ uncertainty.

non-polar surface waters (between 40°S and 50°N in the Atlantic or 40°N in the Pacific). t_{proj} in this case provides a measure of the time lag for the entrainment of surface waters from the non-polar surface region to the polar deep waters. Our calculated t_{proj} of the Drake Passage shows that ventilation ages have a rather small variability in the well-resolved records, with the exception of those reconstructed at Sars Seamount over the Holocene (Methods). The sites with only a few coral samples across the Holocene (Burdwood Bank, Cape Horn and the Shackleton Fracture Zone) also show limited variability of t_{proj} , which fits well into the modern ^{14}C ventilation structure in the Southern Ocean²¹. t_{proj} at Sars Seamount indicates that ventilation was better during the early Holocene (10.5–7.5 ka) than the later Holocene. Strongly ventilated signatures at ~ 9.6 ka have been recorded by corals at a water depth of 692 m, with radiocarbon contents as high as those typically only observed in thermocline waters at Burdwood Bank and Cape Horn. The ventilation age at Sars Seamount of ~ 9.6 ka appears to be even younger than that of the northern site (Burdwood Bank) at similar depths during the early Holocene (Fig. 3). During ~ 6.8 – 1.6 ka, available data from a water depth of 647–981 m at Sars Seamount show that t_{proj} was fairly stable at 643 ± 103 years ($n = 6$; 2σ ; Fig. 3). In general, the standard deviations of t_{proj} at each site are close to or smaller than the 2σ uncertainties of Marine20 (~ 110 – 150 years in the Holocene). Similarly, records from the Reykjanes Ridge site exhibit essentially invariant ventilation ages ($\sim 20 \pm 82$ years; $n = 17$; 2σ).

Impact of climate forcing on polar ocean overturning

Previous reconstructions of radiocarbon from the near-shore Northeast Atlantic indicate well-ventilated mid-depth waters during the Holocene

similar to the pre-bomb modern time^{22,23} (Fig. 3). However, those records exhibit larger short-term variability compared with our samples from Reykjanes Ridge, which sits in the centre of the deep subpolar gyre. The present-day deep waters recorded by Reykjanes Ridge corals at water depths of ~ 1.3 – 1.4 km were primarily formed via the Labrador Sea Water (LSW) convection with mixing of Northeast Atlantic Deep Water²⁴. Northeast Atlantic Deep Water itself reflects mixing between LSW, Iceland–Scotland Overflow Water and modified Antarctic bottom waters²⁵. Therefore, our studied site at Reykjanes Ridge represents an ideal location for recording average North Atlantic Deep Water (NADW) signatures. Compensating feedbacks might have existed in the process of NADW formation through subpolar gyre modulation on the intensity of LSW convection and Iceland–Scotland Overflow Water^{13,26}. For example, during weak LSW convection in response to enhanced melt water flux, the mixing of such fresh components into the polar North Atlantic might be decreased, thus enhancing deep-water formation in the Norwegian Sea^{13,26}. Our North Atlantic deep-sea coral $\Delta^{14}\text{C}$ evolution is essentially identical to that of Marine20, suggesting that deep waters overflowing the Reykjanes Ridge had not experienced any prolonged time of isolation (that is, multi-centennial) after sinking from the surface at our sampled resolution. Notably, the difference in the average t_{proj} between 9.7–7.9 and 5.8–2.2 ka is only 5 ± 82 years ($n = 10$; 2σ). This exceptionally constant t_{proj} suggests that the long-term strength of North Atlantic overturning circulation was invariant during the Holocene. These results are also consistent with independent proxy studies from high-resolution $^{231}\text{Pa}/^{230}\text{Th}$ measurements of North Atlantic detrital sediment cores^{10,11} through this time period (Fig. 3c).

In the Southern Ocean, the transport of deep waters towards the surface is related to the upwelling of Upper Circumpolar Deep Water (UCDW) and the lower overturning cell linked to Antarctic Bottom Water upwelling²⁴. At shallower depths, the upwelled UCDW is ventilated through air–sea gas exchange, mixes with well-ventilated subtropical waters and transforms into intermediate and mode waters²⁴. The Drake Passage is a unique geographical location of the Southern Ocean where the meridional extent of the Antarctic Circumpolar Current (ACC) converges between South America and the Antarctic Peninsula. What then caused the distinct changes in t_{proj} at Sars Seamount but not the other sites during the early Holocene? Sars Seamount is located close to the modern polar front that approximately divides the downwelling of well-ventilated surface waters and the upwelling of relatively poorly ventilated UCDW in the upper ocean²⁴ (Fig. 4a). This unique location makes Sars Seamount more sensitive to shifts in the polar front and conditions in the Antarctic zone compared with the other locations. We suggest that better ventilation at Sars Seamount is consistent with a more poleward position of the polar front during the early Holocene compared with the later period. In this case, downwelling of the upper ocean waters would occur at more southern latitudes along with poleward polar front migration, thus leading to enhanced ventilation at Sars Seamount (Fig. 4). Indeed, recent studies based on radiolarian and diatom assemblages from the Indian sector of the Southern Ocean^{27,28} have indicated poleward polar front migration by a few degrees during the early Holocene.

However, strong ventilation recorded by Sars Seamount during ~ 9.6 ka is even better than the northern sites at similar depths, requiring increased mixing of ^{14}C -enriched water from the south as well. Higher ice-rafted debris flux from the Antarctic to the Scotia Sea (Fig. 3d) during the early Holocene may reflect higher fresh water input to the Antarctic Zone. These (sub)millennial forcings could potentially result in a transient response of the Southern Ocean ventilation and contribute to the higher radiocarbon content observed at Sars Seamount. For example, transient input of western Antarctic ice-sheet melt associated with rapid deglaciation at ~ 9.6 ka (ref. 29) could result in strong stratification and thus a longer residence time and enhanced air–sea gas exchange of the Antarctic surface waters, which could then be mixed on isopycnals down to the depths of the Sars Seamount site

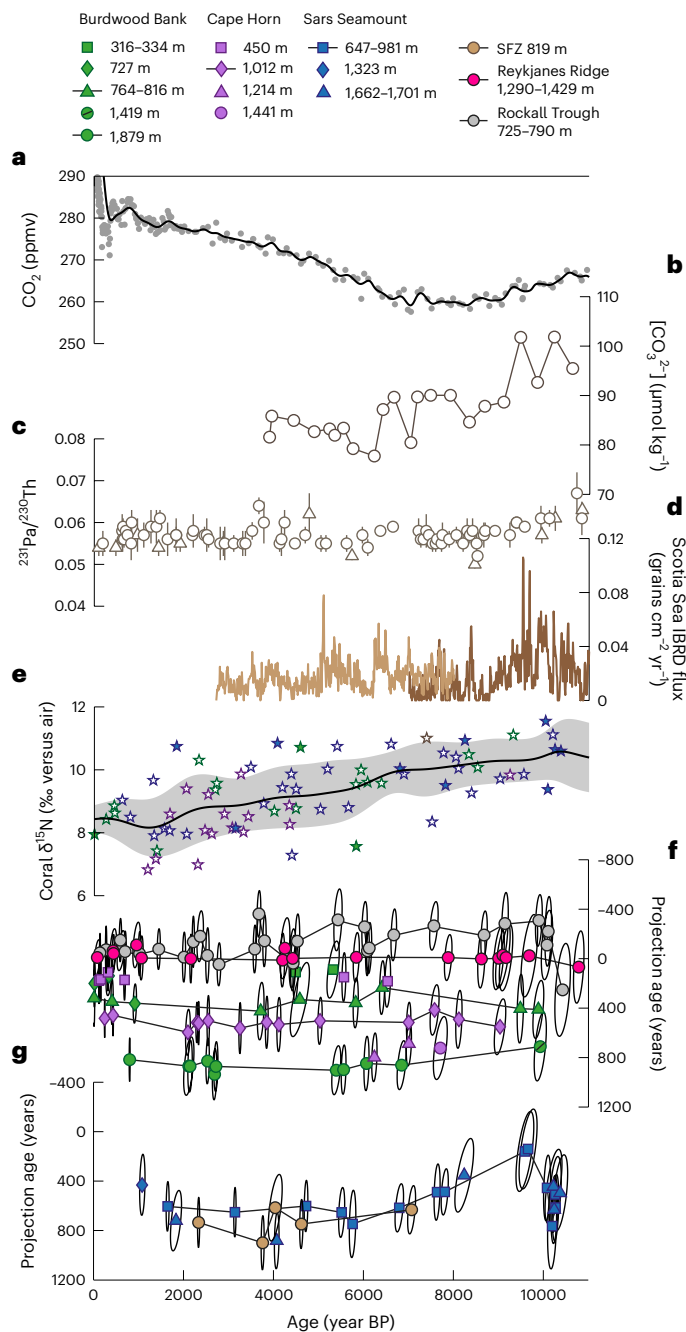


Fig. 3 | Reconstructed t_{proj} from this study compared with other atmosphere and ocean records. a, Atmospheric $p\text{CO}_2$ recorded in the European Project for Ice Coring in Antarctica Dome C ice core². **b**, Seawater CO_3^{2-} concentration based on B/Ca of benthic foraminifera at a water depth of 4 km in the Indian Ocean³⁵. **c**, Sedimentary $^{231}\text{Pa}/^{230}\text{Th}$ from the deep North Atlantic—a proxy of AMOC strength¹¹. **d**, Stacks of the iceberg-rafted debris (IBRD) from the Scotia Sea^{4,50}. **e**, Nitrogen isotopes ($\delta^{15}\text{N}$)—a proxy of surface water N utilization—recorded within the deep-sea coral skeleton from Burdwood Bank (green), Cape Horn (purple) and Sars Seamount (blue)⁵¹. Empty symbols represent samples with reconnaissance ^{14}C ages, whereas filled symbols represent samples with U-series ages. The black line with shading denotes the smoothed record with 2σ uncertainties. **f**, t_{proj} of different depths of Burdwood Bank, Cape Horn, Reykjanes Ridge and Rockall Trough^{22,23} to the northwest of Scotland. **g**, t_{proj} at the Sars Seamount and Shackleton Fracture Zone sites. The errors associated with U-series ages, ^{14}C dating and uncertainties of Marine20 have all been propagated and are shown as $\pm 2\sigma$ error ellipses. The symbols of ^{14}C data in **f** and **g** follow Figs. 1 and 2.

(Fig. 4c). Nevertheless, the near-constant ventilation gradient between records from the North Atlantic and the Southern Ocean, as well as the lack of any long-term trend in t_{proj} at each site except Sars Seamount, provide strong support that Southern Ocean overturning remained stable without prolonged, large-scale disturbance. Likewise, reported coral Nd isotope data³⁰ also show limited variability at each site of the Drake Passage through the Holocene, with the exception of two data points in the middle Holocene. These two radiogenic isotope signatures recorded in Sars Seamount corals (869 m) could be related to zonal mixing of more radiogenic waters from the Pacific rather than changes in large-scale meridional overturning. Given that the t_{proj} of the deep UCDW, as represented by the deepest samples from Burdwood Bank (Fig. 1), is 870 ± 67 years ($n = 10$; 2σ ; that is, $<10\%$ variability), the variability of the mixing proportion between well-ventilated North Atlantic and poorly ventilated Pacific endmembers should also have been similarly small during the Holocene. Our study could not exclude the possibility of strong short-term AMOC slowdown following major melt water pulses during the Holocene (for example, the 8.2 ka event³¹ and other interglacials³²). Given the rapid sea-level rise and thus ice-sheet decay in the early Holocene, our study supports assertions derived from a conceptual framework, which suggests that AMOC reaches a stable strong mode once atmospheric CO_2 levels approach pre-industrial levels (that is, regardless of the changes in Northern Hemisphere ice-sheet volume)^{33,34}.

Decoupling between circulation and biogeochemical cycles

The stability of the millennial polar ocean overturning leads us to suggest that the long-term Holocene $p\text{CO}_2$ evolution was not the result of changing ocean overturning circulation. In particular, during the major phase of rising atmospheric $p\text{CO}_2$ (for example, 7–2 ka), none of our deep records show any sign of ventilation changes (Fig. 3), suggesting that overturning in the North Atlantic and Southern Ocean did not drive changes in oceanic carbon release during this period. While our study does not provide additional constraints on oceanic biogeochemical cycles, proxies suggest that carbon and nutrient distribution within the water column was not in a steady state over the Holocene. For example, deep oceanic $[\text{CO}_3^{2-}]$ content shows a prominent decrease in the early Holocene (Fig. 3b), indicating ocean alkalinity removal and the release of carbon to the atmosphere³⁵. Foraminiferal boron isotopes also suggest a high $\Delta p\text{CO}_2$ relative to the contemporaneous atmosphere in surface waters of the Subantarctic Zone and Eastern Equatorial Pacific in the early Holocene, potentially as a result of carbon release via continuous Circumpolar Deep Water upwelling and intermediate water advection³⁶. In contrast, nitrogen isotope (for example, Fig. 3e) and productivity records from the northern Antarctic Zone indicate a gradually decreased nutrient utilization rate and increased nutrient supply towards the late Holocene⁶, inferred to be associated with obliquity-driven enhanced westerlies and Southern Ocean overturning³⁷. We surmise that the $\delta^{15}\text{N}$ decrease in diatom or coral-bound organic matter observed in the northern Antarctic Zone is probably the result of nutrient redistribution within the ocean basins following deglaciation, rather than increased physical overturning. It has long been hypothesized and modelled that the redistribution of major denitrification locations (for example, between the continental shelf sediments and the deep sea) could affect global biogeochemical cycles³⁸. The sites of denitrification and corresponding N_2 fixation could change as a result of sea-level rise³⁹ and oxygen availability⁴⁰ in the upper ocean, which are not directly dependent on meridional overturning circulation. For example, a decrease in bulk sediment $\delta^{15}\text{N}$ values of the eastern tropical Pacific over the past 10,000 years may partly reflect decreased denitrification in response to a weakened oxygen minimum zone⁴¹. In turn, decreased denitrification in the eastern Pacific water column might effectively increase the nitrate concentration and decrease the $\delta^{15}\text{N}$ of the deep Pacific returning flow to the Southern

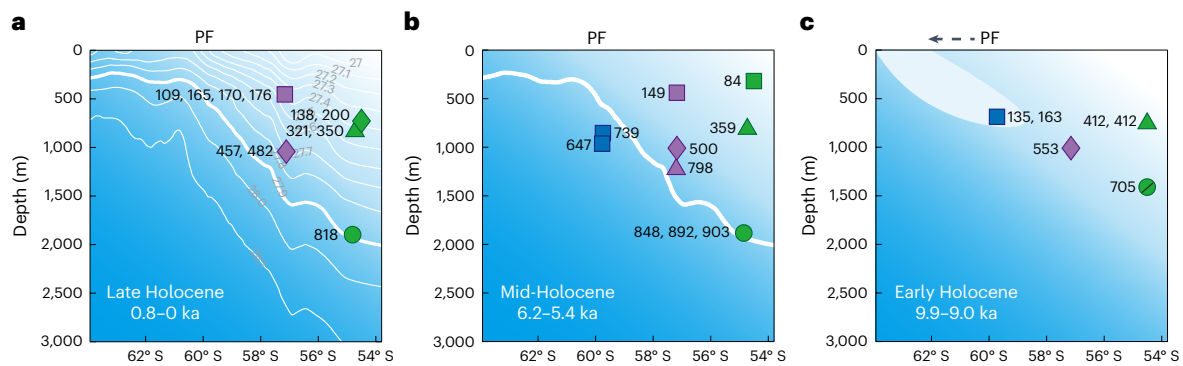


Fig. 4 | Meridional distribution of t_{proj} across the Drake Passage during the late, middle and early Holocene. a–c, Meridional distribution of t_{proj} (years) across the Drake Passage during the late (a), middle (b) and early Holocene (c). Multiple age numbers along a single symbol indicate multiple samples from the same location during each period. The white lines in a illustrate the modern neutral density anomalies (GLODAPv2.2019; ref. 49).

Lighter background colour illustrates a younger ventilation age. The black dashed arrow indicates the inferred southward migration of the polar front (PF) in the early Holocene. The light blue area at the top of c denotes transiently enhanced mixing of the ^{14}C -enriched signatures from the surface ocean in the early Holocene, probably associated with southward polar front migration and enhanced air–sea gas exchange.

Ocean. Other factors, such as changes in the efficiency of nutrient recycling in the upper water column (for example, associated with the depth of organic particle remineralization or ecological community structure) also warrant investigation⁴², which is beyond the scope of our study. These nutrient redistribution processes do not require large changes in oceanic N inventory over the Holocene. Future work should target records from more southern latitudes of the Antarctic Zone to quantitatively understand the contribution of these processes to the Holocene biogeochemical cycles.

Other than changes in oceanic biogeochemical cycles, variability in land carbon inventory is also probably important, as supported by transient carbon cycle modelling⁴³, as well as archaeological and ecological evidence (for example, refs. 44,45) during the Holocene. Closing the Holocene atmosphere carbon budget would require a better understanding of natural and human-associated changes in terrestrial organic carbon stock^{46,47}. In essence, if orbital parameters alone are sufficient to predict CO_2 evolution during the Holocene, we would expect the atmosphere p_{CO_2} to decrease continuously like its closest analogue, Marine Isotope Stage 19c (ref. 48). While such a trend is not observed, the exact mechanism of Holocene atmosphere p_{CO_2} evolution remains an open question. In any case, our deep-sea coral ^{14}C data based on precise, absolute U-series ages provide tight constraints on the stability of the polar ocean overturning and thus demonstrate a clear decoupling between physical ocean circulation and atmospheric p_{CO_2} in the Earth's most recent interglacial period.

Online content

Any methods, additional references, Nature Portfolio reporting summaries, source data, extended data, supplementary information, acknowledgements, peer review information; details of author contributions and competing interests; and statements of data and code availability are available at <https://doi.org/10.1038/s41561-023-01214-2>.

References

- Bond, G. et al. A pervasive millennial-scale cycle in North Atlantic Holocene and glacial climates. *Science* **278**, 1257–1266 (1997).
- Lamy, F. et al. Holocene changes in the position and intensity of the southern westerly wind belt. *Nat. Geosci.* **3**, 695–699 (2010).
- Saunders, K. M. et al. Holocene dynamics of the Southern Hemisphere westerly winds and possible links to CO_2 outgassing. *Nat. Geosci.* **11**, 650–655 (2018).
- Bakker, P., Clark, P. U., Gollidge, N. R., Schmittner, A. & Weber, M. E. Centennial-scale Holocene climate variations amplified by Antarctic Ice Sheet discharge. *Nature* **541**, 72–76 (2017).
- Moreno, P. I., Francois, J. P., Moy, C. M. & Villa-Martinez, R. Covariability of the Southern Westerlies and atmospheric CO_2 during the Holocene. *Geology* **38**, 727–730 (2010).
- Studer, A. S. et al. Increased nutrient supply to the Southern Ocean during the Holocene and its implications for the pre-industrial atmospheric CO_2 rise. *Nat. Geosci.* **1**, 756–760 (2018).
- Monnin, E. et al. Evidence for substantial accumulation rate variability in Antarctica during the Holocene, through synchronization of CO_2 in the Taylor Dome, Dome C and DML ice cores. *Earth Planet. Sci. Lett.* **224**, 45–54 (2004).
- Thornalley, D. J. R. et al. Long-term variations in Iceland–Scotland overflow strength during the Holocene. *Clim. Past* **9**, 2073–2084 (2013).
- Kissel, C., Van Toer, A., Laj, C., Cortijo, E. & Michel, E. Variations in the strength of the North Atlantic bottom water during Holocene. *Earth Planet. Sci. Lett.* **369**, 248–259 (2013).
- Hoffmann, S. S., McManus, J. F. & Swank, E. Evidence for stable Holocene basin-scale overturning circulation despite variable currents along the deep western boundary of the North Atlantic Ocean. *Geophys. Res. Lett.* **45**, 13427–13436 (2018).
- Lippold, J. et al. Constraining the variability of the Atlantic Meridional Overturning Circulation during the Holocene. *Geophys. Res. Lett.* **46**, 11338–11346 (2019).
- Ayache, M., Swingedouw, D., Mary, Y., Eynaud, F. & Colin, C. Multi-centennial variability of the AMOC over the Holocene: a new reconstruction based on multiple proxy-derived SST records. *Glob. Planet. Change* **170**, 172–189 (2018).
- Thornalley, D. J. R., Elderfield, H. & McCave, I. N. Holocene oscillations in temperature and salinity of the surface subpolar North Atlantic. *Nature* **457**, 711–714 (2009).
- Repschlager, J., Garbe-Schonberg, D., Weinelt, M. & Schneider, R. Holocene evolution of the North Atlantic subsurface transport. *Clim. Past* **13**, 333–344 (2017).
- Buckley, M. W. & Marshall, J. Observations, inferences, and mechanisms of the Atlantic Meridional Overturning Circulation: a review. *Rev. Geophys.* **54**, 5–63 (2016).
- Varma, V. et al. Holocene evolution of the Southern Hemisphere westerly winds in transient simulations with global climate models. *Clim. Past* **8**, 391–402 (2012).
- Skinner, L. C. & Bard, E. Radiocarbon as a dating tool and tracer in paleoceanography. *Rev. Geophys.* **60**, e2020RG000720 (2022).

18. Reimer, P. J. et al. The IntCal20 Northern Hemisphere radiocarbon age calibration curve (0–55 cal kyr BP). *Radiocarbon* **62**, 725–757 (2020).
19. Galbraith, E. D., Kwon, E. Y., Bianchi, D., Hain, M. P. & Sarmiento, J. L. The impact of atmospheric $p\text{CO}_2$ on carbon isotope ratios of the atmosphere and ocean. *Glob. Biogeochem. Cycles* **29**, 307–324 (2015).
20. Heaton, T. J. et al. Marine20—the marine radiocarbon age calibration curve (0–55,000 cal BP). *Radiocarbon* **62**, 779–820 (2020).
21. Key, R. M. et al. A global ocean carbon climatology: results from Global Data Analysis Project (GLODAP). *Glob. Biogeochem. Cycles* **18**, GB4031 (2004).
22. Frank, N. et al. Eastern North Atlantic deep-sea corals: tracing upper intermediate water $\Delta^{14}\text{C}$ during the Holocene. *Earth Planet. Sci. Lett.* **219**, 297–309 (2004).
23. Colin, C. et al. Millennial-scale variations of the Holocene North Atlantic mid-depth gyre inferred from radiocarbon and neodymium isotopes in cold water corals. *Quat. Sci. Rev.* **211**, 93–106 (2019).
24. Talley, L. D. *Descriptive Physical Oceanography: An Introduction* (Academic Press, 2011).
25. Lacan, F. & Jeandel, C. Acquisition of the neodymium isotopic composition of the North Atlantic Deep Water. *Geochem. Geophys. Geosyst.* **6**, Q12008 (2005).
26. Hatun, H., Sando, A. B., Drange, H., Hansen, B. & Valdimarsson, H. Influence of the Atlantic subpolar gyre on the thermohaline circulation. *Science* **309**, 1841–1844 (2005).
27. Civel-Mazens, M. et al. Antarctic Polar Front migrations in the Kerguelen Plateau region, Southern Ocean, over the past 360 kyrs. *Glob. Planet Change* **202**, 103526 (2021).
28. Ghadi, P. et al. Antarctic sea-ice and palaeoproductivity variation over the last 156,000 years in the Indian sector of Southern Ocean. *Mar. Micropaleontol.* **160**, 101894 (2020).
29. Bentley, M. J. et al. Rapid deglaciation of Marguerite Bay, western Antarctic Peninsula in the Early Holocene. *Quat. Sci. Rev.* **30**, 3338–3349 (2011).
30. Struve, T., Wilson, D. J., van de Flierdt, T., Pratt, N. & Crockett, K. C. Middle Holocene expansion of Pacific Deep Water into the Southern Ocean. *Proc. Natl Acad. Sci. USA* **117**, 889–894 (2020).
31. Kleiven, H. F. et al. Reduced North Atlantic Deep Water coeval with the glacial Lake Agassiz freshwater outburst. *Science* **319**, 60–64 (2008).
32. Galaasen, E. V. et al. Interglacial instability of North Atlantic Deep Water ventilation. *Science* **367**, 1485–1489 (2020).
33. Zhang, X., Knorr, G., Lohmann, G. & Barker, S. Abrupt North Atlantic circulation changes in response to gradual CO_2 forcing in a glacial climate state. *Nat. Geosci.* **10**, 518–523 (2017).
34. Barker, S. & Knorr, G. Millennial scale feedbacks determine the shape and rapidity of glacial termination. *Nat. Commun.* **12**, 2273 (2021).
35. Yu, J. M. et al. Loss of carbon from the deep sea since the Last Glacial Maximum. *Science* **330**, 1084–1087 (2010).
36. Martinez-Boti, M. A. et al. Boron isotope evidence for oceanic carbon dioxide leakage during the last deglaciation. *Nature* **518**, 219–222 (2015).
37. Ai, X. Y. E. et al. Southern Ocean upwelling, Earth’s obliquity, and glacial–interglacial atmospheric CO_2 change. *Science* **370**, 1348–1352 (2020).
38. Christensen, J. P. Carbon export from continental shelves, denitrification and atmospheric carbon dioxide. *Cont. Shelf Res.* **14**, 547–576 (1994).
39. Ren, H. J. et al. Impact of glacial/interglacial sea level change on the ocean nitrogen cycle. *Proc. Natl Acad. Sci. USA* **114**, E6759–E6766 (2017).
40. Galbraith, E. D. et al. The acceleration of oceanic denitrification during deglacial warming. *Nat. Geosci.* **6**, 579–584 (2013).
41. Thunell, R. C. & Kepple, A. B. Glacial-Holocene $\delta^{15}\text{N}$ record from the Gulf of Tehuantepec, Mexico: implications for denitrification in the eastern equatorial Pacific and changes in atmospheric N_2O . *Glob. Biogeochem. Cycles* **18**, GB1001 (2004).
42. Kwon, E. Y., Primeau, F. & Sarmiento, J. L. The impact of remineralization depth on the air–sea carbon balance. *Nat. Geosci.* **2**, 630–635 (2009).
43. Menviel, L. & Joos, F. Toward explaining the Holocene carbon dioxide and carbon isotope records: results from transient ocean carbon cycle-climate simulations. *Paleoceanography* **27**, PA1207 (2012).
44. Roberts, N. et al. Europe’s lost forests: a pollen-based synthesis for the last 11,000 years. *Sci. Rep.* **8**, 716 (2018).
45. Stephens, L. et al. Archaeological assessment reveals Earth’s early transformation through land use. *Science* **365**, 897–902 (2019).
46. Kaplan, J. O. et al. Holocene carbon emissions as a result of anthropogenic land cover change. *Holocene* **21**, 775–791 (2010).
47. Erb, K.-H. et al. Unexpectedly large impact of forest management and grazing on global vegetation biomass. *Nature* **553**, 73–76 (2018).
48. Tzedakis, P. C., Channell, J. E. T., Hodell, D. A., Kleiven, H. F. & Skinner, L. C. Determining the natural length of the current interglacial. *Nat. Geosci.* **5**, 138–141 (2012).
49. Olsen, A. et al. GLODAPv2.2019—an update of GLODAPv2. *Earth Syst. Sci. Data* **11**, 1437–1461 (2019).
50. Weber, M. E. et al. Millennial-scale variability in Antarctic ice-sheet discharge during the last deglaciation. *Nature* **510**, 134–138 (2014).
51. Wang, X. T. et al. Deep-sea coral evidence for lower Southern Ocean surface nitrate concentrations during the last ice age. *Proc. Natl Acad. Sci. USA* **114**, 3352–3357 (2017).

Publisher’s note Springer Nature remains neutral with regard to jurisdictional claims in published maps and institutional affiliations.

Open Access This article is licensed under a Creative Commons Attribution 4.0 International License, which permits use, sharing, adaptation, distribution and reproduction in any medium or format, as long as you give appropriate credit to the original author(s) and the source, provide a link to the Creative Commons license, and indicate if changes were made. The images or other third party material in this article are included in the article’s Creative Commons license, unless indicated otherwise in a credit line to the material. If material is not included in the article’s Creative Commons license and your intended use is not permitted by statutory regulation or exceeds the permitted use, you will need to obtain permission directly from the copyright holder. To view a copy of this license, visit <http://creativecommons.org/licenses/by/4.0/>.

© The Author(s) 2023

Methods

Samples and site descriptions

The Drake Passage samples were dredged from a number of sites (Burdwood Bank, Cape Horn, Sars Seamount and the Shackleton Fracture Zone) during RVIB *Nathaniel B. Palmer Cruises* 0805 and 1103 in 2008 and 2011, respectively. Sixteen Holocene samples have been reported previously in discussions of the deglacial Southern Ocean ventilation⁵². In this Article, we provide a spatially and temporally detailed ¹⁴C ventilation picture of the Holocene by presenting 61 new Drake Passage data points. Our study thus avoids ambiguities in assessing ventilation changes caused by linking deep-sea coral samples from different depths and sites. These Holocene samples were selected based on reconnaissance dating^{53,54} of more than 1,500 samples and the preservation of coral skeletons. The species of the samples are mostly solitary coral *Desmophyllum* with a few other genera such as *Flabellum*, *Balanophyllia* and *Caryophyllia*.

A series of frontal zones where the ACC is most enhanced are confined within the Drake Passage²⁴. In the upper water column of the Drake Passage (water depth <2.0 km), the most prominent water mass is the UCDW, which is identified by its low oxygen content (<180 μmol kg⁻¹) (ref. 24), with a Δ¹⁴C of about -140 to -160‰. Despite large Δ¹⁴C differences between the Pacific and Atlantic on the same isopycnal surfaces in the deep waters, the horizontal and vertical mixings have effectively homogenized ¹⁴C once these waters have been steered into the ACC²¹. Note that our coral samples did not directly record Antarctic Bottom Water signatures. However, unlike conservative tracers used to study ocean circulation, ¹⁴C is particularly sensitive to the aging of the deep waters due to radioactive decay. The upper North Atlantic overturning cell and lower Antarctic bottom water overturning cell are intertwined through the circumpolar deep waters. Today, the UCDW originates from mixing between deep waters from the Pacific, Indian and Atlantic oceans. Overlying the UCDW is the downwelling Antarctic Intermediate Water, which has lower salinity and a higher oxygen concentration, while the overlying mode water is characterized by its low nutrient concentration, such as silicon (for example, <10 μmol kg⁻¹) (ref. 55). When the overturning rate in the Antarctic bottom cell slows down, the Pacific and Indian deep waters become aged and the ¹⁴C signatures of UCDW and Antarctic Intermediate Water would change accordingly. Similarly, decreased transport of well-ventilated North Atlantic deep waters into the circumpolar deep waters would also cause aging of the ¹⁴C recorded by Drake Passage corals. Therefore, ¹⁴C recorded by our samples provides a unique tracer that can be used to monitor the rate of global meridional overturning circulation.

The North Atlantic samples were dredged from the Reykjanes mid-ocean ridge at a depth range of -1,290–1,429 m during *Celtic Explorer* cruise CE0806 in 2008. These fossil samples are mostly framework-building corals (*Lophelia pertusa* and *Madrepora oculata*). The water mass where these corals were grown is part of the subpolar gyre circulation system, characterized by cyclonic re-circulation steered by the topographic boundaries in the mid-depths⁵⁶. The modern ventilation of waters at our studied depth is mainly via Labrador Sea convection along with potential mixing of intermediate waters of subtropical origin⁵⁷. Pre-bomb Δ¹⁴C distribution during the late nineteenth and early twentieth centuries of North Atlantic deep waters is helpful to understand the data of our study. The surface Δ¹⁴C along the northeast Atlantic coast is around -45 ± 5‰ based on shells of known age⁵⁸. In the intermediate waters at 697 m in the Bay of Biscay, deep-sea corals show a mean Δ¹⁴C value of around -59‰, with quasi-decadal oscillations of -15‰ (ref. 59). Relatively ¹⁴C-depleted intermediate waters (for example, Δ¹⁴C down to -100‰) are found in the low-latitude subtropical intermediate waters of Antarctic origin²¹. These waters might be shoaled to the subsurface along the North American continental margin⁶⁰. Coral records suggest that convective mixing in the Labrador Sea can effectively homogenize the pre-bomb Δ¹⁴C signature (-67 ± 4‰) in the Northwest Atlantic at least to -1 km depth⁶⁰. As a result, the subsurface waters of the subpolar North Atlantic are

well ventilated with relatively homogenous pre-bomb ¹⁴C signatures. Therefore, ¹⁴C in our Holocene samples can be understood as mixing between the ¹⁴C-enriched surface North Atlantic waters and potentially ¹⁴C-depleted intermediate waters of southern origin at periods of decreased AMOC.

U-series analytical methods

U-series dating of the deep-sea corals with the isotope spiking method was performed by the Bristol Isotope Group at the University of Bristol. Chen et al.⁶¹ have described the procedure for column chemistry and mass spectrometry in the U-series analysis of deep-sea corals in detail, which we followed in this study. All samples were physically and chemically cleaned after cutting about 0.2–1.0 g of chunky aragonite from each of the deep-sea coral specimens. Approximately 0.2 g of each sample was dissolved in optima-grade HNO₃ and spiked with -0.06 g of the ²³⁶U–²²⁹Th mixed spike. To facilitate column chemistry, U and Th in the sample were first co-precipitated with iron hydroxides and then dissolved and loaded to anion-exchange columns to further purify the U and Th fractions. U and Th isotopes were measured using the sample-standard bracketing method on a Neptune multi-collector inductively coupled plasma mass spectrometer. The typical internal precision for ²³⁴U/²³⁸U is -0.7–1‰ and for ²²⁹Th/²³⁰Th it is -0.9–1.5‰, with accuracy better than 1 and 2‰, respectively. To maintain consistency with previously published coral age data, we adopted the decay constants of the U-series nuclides from Cheng et al.⁶². Analytical errors and procedural blanks were propagated analytically into the isotope ratios of ²³⁴U/²³⁸U, ²³⁶U/²³⁸U and ²²⁹Th/²³⁰Th. An additional source of uncertainty for age determination is the initial ²³⁰Th incorporated into the coral skeleton. The initial [²³⁰U/²³²Th] values of the Drake Passage and North Atlantic corals are assumed to be 37 ± 37 (2σ) and 14.8 ± 14.8 (2σ), respectively^{51,63}. A Monte Carlo technique was then applied to propagate the errors of isotope ratios into the final age uncertainties.

Radiocarbon analysis and data report

Approximately 15–20 mg of cleaned sample was weighed and leached by 0.1 N HCl to -10 mg before graphitization in an automated graphitization device. The graphite target was analysed at the new MICADAS Accelerator Mass Spectrometer (AMS) facility at the University of Bristol. Before our sample analysis, the consistency of the coral ¹⁴C data measured by the Bristol AMS facility had been checked with repeated measurements of coral samples that were previously analysed in the AMS laboratory of the University of California, Irvine⁶⁴. The fossil corals with ages older than 100 ka yielded a ¹⁴C age of 46–50 ka and were used as the procedural blank. All data reported in this study have been δ¹³C and blank corrected, as shown in Supplementary Table 1.

There are various ways to estimate the past oceanic ¹⁴C ventilation based on combined U-series dating and ¹⁴C analysis of deep corals. Δ¹⁴C is a straightforward measure of the actual ¹⁴C content in past seawater, which is calculated as: Δ¹⁴C_{coral} = (F¹⁴C × e^(calendar age/8,267) - 1) × 1,000. The projection age is also a common way to report deep-ocean ¹⁴C data^{65,66}. Changes in atmospheric ¹⁴C levels take time to affect the surface ocean, and the mixing between the surface layer and the deeper ocean layers would result in effective signal damping²⁰. This effect causes changes in atmospheric ¹⁴C levels to be smoothed and shifted in phase in the surface ocean. When applying ¹⁴C as a deep circulation tracer, it can be assumed that deep-water ¹⁴C is sourced from surface waters. Therefore, we project our data to Marine20 to account for the effect of surface oceanic smoothing of atmospheric ¹⁴C. Marine20 used for projection age calculation was obtained from a large set of simulations with various ocean–atmosphere–biosphere parameterizations of the global carbon cycle²⁰. The simulations using the BICYCLE box model⁶⁷ were forced by IntCal20 atmosphere ¹⁴C and ice-core p_{CO₂} data, incorporating effects related to changes in ocean mixing and air–sea gas exchange. Marine20 thus serves as the ideal candidate for initial Δ¹⁴C of surface source waters that supply the deep and polar oceans. The negative

projection age of the sample, in this case, would mean a higher $\Delta^{14}\text{C}$ in the coral record than in the Marine20 curve of the same age, while it would take $|t_{\text{proj}}|$ for the sample ^{14}C decay trajectory to intersect with Marine20. The calculated mean Holocene t_{proj} values are -20 ± 82 ($n = 17$; 2σ), 159 ± 54 ($n = 6$; 2σ), 335 ± 121 ($n = 6$; 2σ), 512 ± 92 ($n = 14$; 2σ) and 870 ± 67 years ($n = 10$; 2σ) for Reykjanes Ridge (depth: 1,290–1,429 m), Cape Horn (depth: 450 m), Burdwood Bank (depth: 816 m), Cape Horn (depth: 1,012 m) and Burdwood Bank (depth: 1,879 m), respectively. To avoid attributing modern water masses to past coral locations, we have not grouped samples by modern day water masses as applied in previous deep-sea coral ^{14}C studies⁵². Typically, a single data point (t_{proj}) of the deep-sea corals is thought to average seawater signatures over a few decades. The deep-sea corals grow much slower than the warm water corals. For example, a solitary deep-sea coral with a length of several centimetres has a typical life span of about a century⁶⁸, while the sampling and homogenization of the septa of the coral aragonites would average out over a few decades.

We note that the version of the BICYCLE box model⁶⁷ used to generate Marine20 contains no circulation changes in the Holocene²⁰. If the Holocene atmospheric CO_2 or ^{14}C variability is in part due to ocean circulation changes, the variability will be implicitly included in Marine20. Nevertheless, what makes our dataset unique is the records from multiple sites both in the polar North Atlantic and the Southern Ocean. A stable meridional overturning circulation during the Holocene is necessary not only to maintain the invariant t_{proj} of each site projected to Marine20, but also to ensure stable t_{proj} offsets of different sites in the Southern Ocean from that of NADW (Fig. 2f). The t_{proj} offsets from Reykjanes Ridge for Cape Horn (depth: 450 m), Burdwood Bank (depth: 816 m), Cape Horn (depth: 1,012 m) and Burdwood Bank (depth: 1,879 m) exhibit small variabilities during the Holocene, with values of 179 ± 98 , 355 ± 146 , 532 ± 123 and 890 ± 102 years, respectively (2σ errors propagated). These variabilities are similar to the propagated analytical uncertainties from radiocarbon and U–Th measurements, suggesting that ventilation between these sites has remained constant within proxy uncertainties. In this regard, our conclusion on stable Holocene oceanic overturning does not rely on the accuracy of the Marine20 surface ^{14}C curve.

Data availability

Sample location information, U-series ages and radiocarbon data that support the findings of this study are available from Figshare (<https://doi.org/10.6084/m9.figshare.23455196>).

Code availability

The codes used to calculate $\Delta^{14}\text{C}$ and t_{proj} in this study are available from GitHub (<https://github.com/zeningbaba/radiocarbon.git>).

References

- Burke, A. & Robinson, L. F. The Southern Ocean's Role in carbon exchange during the last deglaciation. *Science* **335**, 557–561 (2012).
- Spooner, P. T., Chen, T., Robinson, L. F. & Coath, C. D. Rapid uranium-series age screening of carbonates by laser ablation mass spectrometry. *Quat. Geochronol.* **31**, 28–39 (2016).
- Burke, A. et al. Reconnaissance dating: a new radiocarbon method applied to assessing the temporal distribution of Southern Ocean deep-sea corals. *Deep Sea Res. Part I Oceanogr. Res. Pap.* **57**, 1510–1520 (2010).
- Ayers, J. M. & Strutton, P. G. Nutrient variability in Subantarctic Mode Waters forced by the Southern Annular Mode and ENSO. *Geophys. Res. Lett.* **40**, 3419–3423 (2013).
- Bower, A. S. et al. Directly measured mid-depth circulation in the northeastern North Atlantic Ocean. *Nature* **419**, 603–607 (2002).
- Lozier, M. S. & Stewart, N. M. On the temporally varying northward penetration of Mediterranean Overflow Water and eastward penetration of Labrador Sea Water. *J. Phys. Oceanogr.* **38**, 2097–2103 (2008).
- Tisnerat-Laborde, N. et al. Variability of the northeast Atlantic sea surface $\Delta^{14}\text{C}$ and marine reservoir age and the North Atlantic Oscillation (NAO). *Quat. Sci. Rev.* **29**, 2633–2646 (2010).
- Montero-Serrano, J. C. et al. Decadal changes in the mid-depth water mass dynamic of the Northeastern Atlantic margin (Bay of Biscay). *Earth Planet. Sci. Lett.* **364**, 134–144 (2013).
- Sherwood, O. A. et al. Late Holocene radiocarbon variability in Northwest Atlantic slope waters. *Earth Planet. Sci. Lett.* **275**, 146–153 (2008).
- Chen, T. et al. Synchronous centennial abrupt events in the ocean and atmosphere during the last deglaciation. *Science* **349**, 1537–1541 (2015).
- Cheng, H. et al. The half-lives of uranium-234 and thorium-230. *Chem. Geol.* **169**, 17–33 (2000).
- Robinson, L. F. et al. Radiocarbon variability in the western North Atlantic during the last deglaciation. *Science* **310**, 1469–1473 (2005).
- Chen, T. et al. Persistently well-ventilated intermediate-depth ocean through the last deglaciation. *Nat. Geosci.* **13**, 733–738 (2020).
- Adkins, J. F. & Boyle, E. A. Changing atmospheric $\Delta^{14}\text{C}$ and the record of deep water paleoventilation ages. *Paleoceanography* **12**, 337–344 (1997).
- Skinner, L. C. & Shackleton, N. J. Rapid transient changes in northeast Atlantic deep water ventilation age across Termination I. *Paleoceanography* **19**, PA2005 (2004).
- Kohler, P., Fischer, H., Munhoven, G. & Zeebe, R. E. Quantitative interpretation of atmospheric carbon records over the last glacial termination. *Glob. Biogeochem. Cycles* **19**, GB4020 (2005).
- Robinson, L. F. et al. The geochemistry of deep-sea coral skeletons: a review of vital effects and applications for palaeoceanography. *Deep Sea Res. Part II Top. Stud. Oceanogr.* **99**, 184–198 (2014).

Acknowledgements

We thank the cruise members of *R/VIB Nathaniel B. Palmer* cruises 0805 and 1103, as well as *Celtic Explorer* cruise CE0806, for supporting the deep-sea coral sampling. T.C. acknowledges support from the Strategic Priority Research Program of Chinese Academy of Sciences (XDB40010200), Fundamental Research Funds for the Central Universities (020614380116) and National Natural Science Foundation of China (41991325, 41822603 and 42021001). L.F.R. acknowledges support from the Natural Environment Research Council (NE/S001743/1, NE/R005117/1, NE/N003861/1 and NE/X00127X/1).

Author contributions

T.C. and L.F.R. designed the study. L.F.R., A.B. and N.J.W. collected the deep-sea coral samples. T.C., T.L., A.B. and T.D.J.K. performed the U-series and radiocarbon analyses. T.C. wrote the manuscript draft, with edits and input from L.F.R., A.B., T.L., X.Z. and the other co-authors. All authors contributed to the discussion on data interpretation.

Competing interests

The authors declare no competing interests.

Additional information

Supplementary information The online version contains supplementary material available at <https://doi.org/10.1038/s41561-023-01214-2>.

Correspondence and requests for materials should be addressed to Tianyu Chen.

Peer review information *Nature Geoscience* thanks Thomas Guilderson and the other, anonymous, reviewer(s) for their contribution to the peer review of this work. Primary Handling Editor: James Super, in collaboration with the *Nature Geoscience* team.

Reprints and permissions information is available at www.nature.com/reprints.